Quantitative Analysis and Interpretation of Dot Echoes Observed with a Doppler Sodar

G. MASTRANTONIO AND J. NAITHANI

Istituto di Fisica dell'Atmosfera, CNR, Rome, Italy

P. S. ANDERSON

British Antarctic Survey, Natural Environment Research Council, Cambridge, United Kingdom

S. ARGENTINI

Istituto di Fisica dell'Atmosfera, CNR, Rome, Italy

I. PETENKO

Institute of Atmospheric Physics, Russian Academy of Sciences, Moscow, Russia

(Manuscript received 23 October 1998, in final form 4 February 1999)

ABSTRACT

While some people involved in the acoustic remote sensing field are aware of the possibility of receiving dot echoes from nonatmospheric targets, most of the papers available in the scientific literature dealing with this phenomenon associate them to atmospheric targets, such as clusters of water vapor inhomogeneity, thermodynamical processes of condensation and reevaporation of water vapor, anisotropic irregularities localized in thin layers, etc. At present, dot echoes are defined by their appearance on the echogram and are not differentiated by causative processes. As such, they share similar characteristics, such as being randomly distributed and having a time length that is similar to the time length of the emitted tone. In this paper dot echoes conforming to this definition are investigated through the analysis of the signal in both the time and frequency domain. The timescale of a dot signature along with the configuration of the sodar system provide an upper limit to the size of the targets producing these echoes. The spectral characteristics and the first and second momenta of the echoes are compared with clear-air echoes as well as with echoes produced by pilot balloons released from nearby sodar antennas. The conclusion is that the dot echoes analyzed in this paper are reflections from birds and are not due to atmospheric effects.

1. Introduction

Cronenwett et al. (1972) first mentioned dot echoes (DTEs) in the acoustic remote sensing literature when they noticed small dotlike traces in the facsimile records during the early morning hours and attributed them to reflections from flying insects. Their interpretation was supported by direct observation of numerous large, flying, long-horned grasshoppers. In successive papers regarding DTE interpretation, this reference has not been quoted. A few years later, Parry et al. (1975), while discussing the interpretation of sounder echoes, explained how ''birds, crickets and individual raindrops produce random dashes or dots on the chart.'' It is clear from the context that the authors are talking about noise, but this can be excluded for ''dot echoes'' since the latter traces disappear from the facsimile record when the pulse emission is switched off. Moreover, the DTE duration appears to be similar to the sounding pulse duration (Petenko and Kallistratova 1996). In 1981, Mingyu et al. reported anomalous echoes on sodar echograms distinct from the conventional atmospheric backscatter, which they termed lump echoes, and which were observed in the neutral atmosphere above the usual sodar structures. A few more cases have been reported elsewhere by other groups (Singal et al. 1985; De et al. 1994; Rao et al. 1995; Vetrov and Ulianov 1996; Vetrov et al. 1998). These echoes have generally been observed in the spring and autumn, around 1900 and 0600 local time and during conditions of stable stratification, light winds, and high humidity. They are observed in association with cold fronts, land–sea breezes, and storms, that is, all situations related with the moisture transport. The names suggested for these isolated echoes are variously ''dot,'' ''lump,'' or ''dash.'' We prefer to des-

Corresponding author address: Giangiuseppe Mastrantonio, IFA/CNR, Via Fosso del Cavaliere 100, 00133 Rome, Italy.
E-mail: gmastro@lux.ifsi.rm.cnr.it

ignate them all as ''dot echoes.'' The interpretation for their origin given by various groups, although varied, rests ultimately on water vapor directly or indirectly, alone or in association with temperature fluctuations. Mingyu et al. (1981) attributed them to density fluctuations caused by the coupled effect of temperature and humidity inhomogeneities. Singal et al. (1985) regarded them to be due to backscattering from temperature and humidity cofluctuations from clusters of water vapor inhomogeneity. Vetrov and Ulianov (1996) observed them both during nighttime as well as daytime over peaks of convective plumes and concluded that they are due to the joint effect of positively correlated temperature and humidity. Rao et al. (1995) associated them with small-scale temperature fluctuations generated in isolated regions by the thermodynamical processes of condensation and reevaporation of water vapor. Their argument was supported by the presence of high water vapor mixing ratio measured by a Raman lidar, which showed large variability at the height of the DTEs. While some groups are able to justify their observations and interpretations through various arguments and complementary datasets, Petenko and Kallistratova (1996) report how the experimental results favor reflection from birds as the origin of DTEs; the scattering cross section is close to typical bird sizes and the observed shapes of the signal are characterized by sharp leading and trailing edges. Lack of visual confirmation led them to hypothesize, in addition, that the observed DTEs may be due to the presence of anisotropic irregularities localized in thin layers. These layers may be able to produce reflections that are stronger than the ones predicted by the theory of scattering by isotropic turbulence. Besides, they rejected humidity as a possible source of this phenomenon since observations were made in mountainous regions where absolute humidity is low.

Similar problems of interpretation of anomalous echoes are faced also by other kinds of active remote sensors. It has been known since World War II that microwave and UHF radars are capable of detecting birds and insects (Larkin 1991; Vaughn 1985). This idea has been exploited since then by ornithologists to study bird migration and other movements (Eastwood 1967; Skolnik 1970; William et al. 1972; Richardson 1976; Gauthreaux 1980; Vaughn 1985) and by entomologists to study the scale and extent of insect activity (Reynolds 1988; Riley 1989) in the lower atmosphere. By 1967–70, the birds and insects became accepted as the primary cause of the ''dot angels'' on radar (Battan 1973; Hardy and Katz 1969; Ottersten 1970). The radar study reveals that there is usually a pronounced diurnal cycle in the aerial density of insects and birds, with a large increase around dusk, which is when many species take off and migrate (William et al. 1972; Riley and Reynolds 1979; Vaughn 1985; Riley 1994). According to these researchers an intense migration of these species occurs at night in the spring and autumn, at which time they climb to several hundred meters and remain in flight for many hours. Insects in particular form discrete dense layers at heights of several hundred meters. These layers are often found to occur at the height of the nocturnal temperature inversion (Vaughn 1985; Riley and Reynolds 1979) or coincide with zones of atmospheric convergence, for example, storm front outflow (Pedgley et al. 1982), with convection, and with sea-breeze fronts (Greenbank et al. 1980; Drake 1982). A similar response of birds to atmospheric layers and local weather systems is reported by William et al. (1972) and Gauthreaux (1980).

The above observations demonstrate the usefulness of active remote sensing to entomological studies; the problem of distinguishing atmospheric and biogenic echoes remains. Jungbluth et al. (1995), O'Bannon (1995), Lee et al. (1995), and Wilczak et al. (1995) have discussed the anomalous wind profiles observed by Doppler radar in comparison with the pilot balloons, particularly after sundown. They identify the vector difference between the pilot balloon and wind profiler as the bird vector. Larkin and Quine (1987, 1989) have identified 11 potential diagnostic variables for distinguishing bird echoes on radar; atmospheric backscatter is more widespread than bird echo and generally has a wider spectral width. The location of the event and the time are important as a bird echo may present a characteristic signature in the same location and possibly at the same time of the day (Larkin and Quine 1989).

The observation density of insects and birds in association with various atmospheric features like convection, nocturnal layers, sea-breeze fronts, cold fronts, etc., by various radar workers are curious enough to warrant scanning the literature once again and rethinking the origin of DTEs or sodar angels (Riley 1994) observed on acoustic radar. The main origin claimed by several authors, that is, the contribution of humidity fluctuations to the acoustic backscattering, may sometimes give unusual echo structures such as the hummocks that are occasionally observed over the sea on the top of thermals (Gaynor and Mandics 1978). In the case of DTEs, however, some doubts may be put forward about their atmospheric origin since no direct association to atmospheric phenomena has been evidenced, and, in most cases, their characteristics have been derived from the visual analysis of facsimile records.

2. Data, site, and processing techniques

Since the late 1970s the authors have collected various relevant sodar data from different sites and during different atmospheric conditions. Campaigns have been carried out over the sea (Fiocco et al. 1980), in continental areas (Greenhut and Mastrantonio 1999), in mountainous terrain (Petenko and Kallistratova 1986), on the tops of high mountains (Fiocco and Mastrantonio 1983), in the vicinities of coasts (Mastrantonio et al. 1994), and in Antarctica (Argentini et al. 1996; Anderson 1996). The frequency and signature of the DTEs

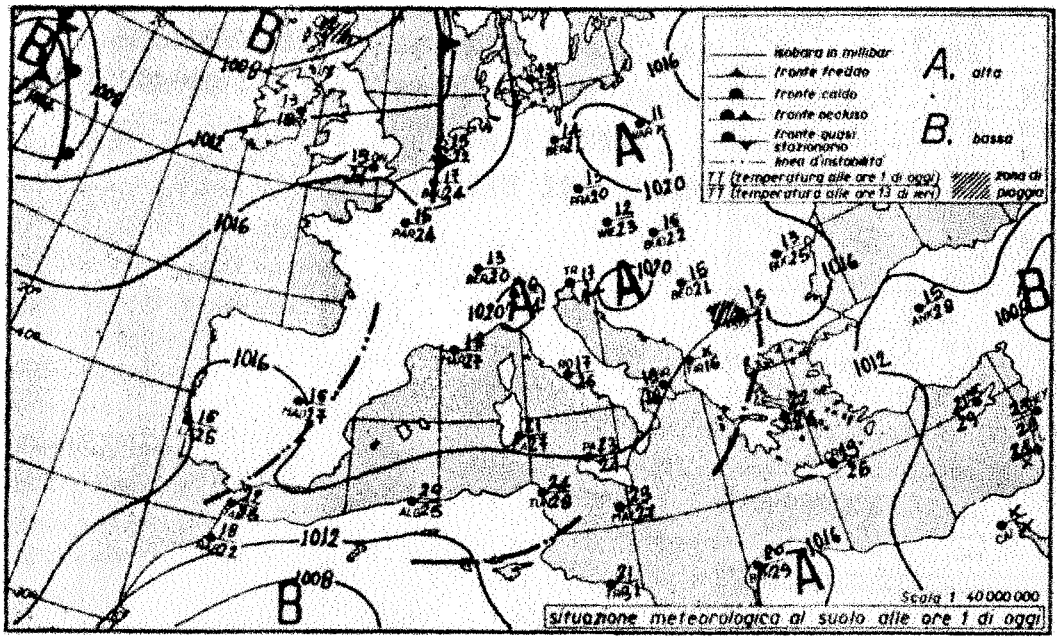

FIG. 1. Meteorological situation surface weather chart, as reported by the Italian Meteo-Service for 0100 LST 7 Sep 1979.

vary considerably depending on the site, local time, and season. DTEs were not noticed during a 2-yr measurement campaign in Dumont d'Urville (Antarctica), during summer campaigns in Terra Nova Bay (Antarctica), at sea, or on the top of the Monte Rosa mountain (4600 m MSL). At the British Antarctic Survey's Halley station (76°S, 26°W), in the south Weddell Sea, DTEs have been recorded by a single-axis monostatic sodar (Anderson 1996). DTEs have also been observed during a 2-yr campaign by several sodars located in Rome and in its surroundings (Mastrantonio et al. 1994). We find a frequency variability of the DTEs depending on the place (more numerous close to the sea and to the city garbage dumps), on the time of the day (more frequent during the evening and night), and on the time of the year (rarely observed during winter season). As for the height of these echoes we find that most of them are located above the ground-based inversion or where thermal turbulence is minimum [see Fig. 1a in Rao et al. (1995)].

Most of the data recorded in the past campaigns are in a format that includes only the instantaneous radial winds, the instantaneous intensity values, and the signal-to-noise information for each range gate for Doppler systems. The sodar configuration commonly used is three divergent monostatic axes. During a campaign in Turbigo (45°32′N, 8°45′E), three acoustic signals (one for each antenna) and a reference frequency were cotemporally recorded on four-track analog magnetic tape. The data were postprocessed to give spectral and time domain characteristics of the echoes. In addition the antenna layout was particularly suitable for studying DTE location; the three vertically pointing antennas were located at the vertices of a right-angled triangle with two sides 100 m long. Details on this campaign may be found in Greenhut and Mastrantonio (1989). Information on the data processing and on the procedures used to get the Doppler information can be found in the papers by Mastrantonio and Fiocco (1982) and Mastrantonio and Argentini (1997). Note that the sodar system was a three-axis monostatic Doppler system, simultaneously radiating 100-ms acoustic bursts at three different frequencies centered around 1818.18 (channel 1), 2000.00 (channel 2), and 1666.66 (channel 3) Hz, respectively, repeating every 6 s. Each antenna was designed around a 2-m diameter parabolic dish reflector, driven by an ALTEC 391E electroacoustic transducer. The three channels had carrier frequencies sufficiently displaced to eliminate cross contamination in the frequency domain. This allows addition of the three signal channels and hence simultaneous digitization. The harmonic analysis of the signal to retrieve the radial wind and spectral width was made with 256 point samples, which corresponds to a height interval of 29 m.

3. Case study from Turbigo on 7 September 1979

In the following, data from one day of the Turbigo campaign are carefully analyzed. During the event, a high pressure system was present and sunny weather was prevalent all over Italy. Figure 1 shows the meteorological situation, as depicted from the Italian Meteorological Service for 0100 local standard time (LST). In particular the high pressure was centered in the mid-

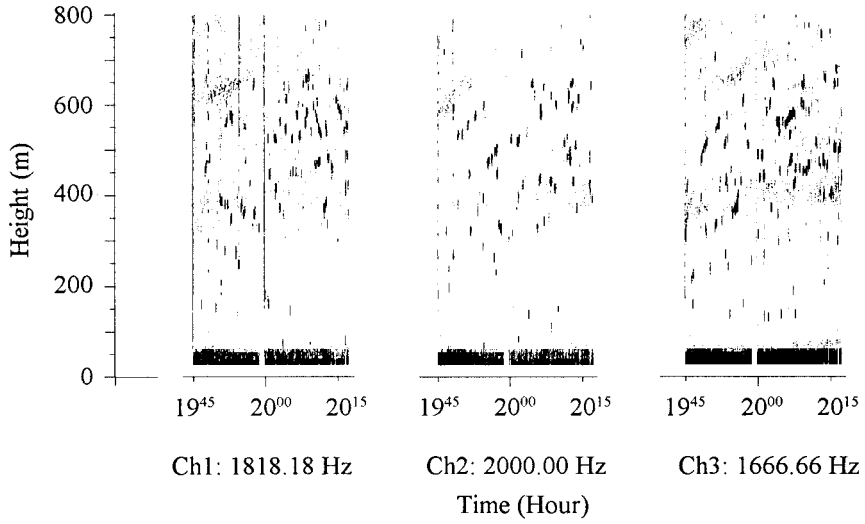

FIG. 2. Echograms recorded by the three antennas for the period used in the present study. Dot echoes are clearly visible together with weak atmospheric echoes due to thermal stratifications.

dle part of Europe, and the background synoptic wind in the northern part of Italy was very weak.

During the campaign, DTEs were observed almost every day, at the same time between 1900 and 2300 LST and at the same height ranges. A time interval has been chosen in which, with numerous DTEs, some thermal turbulence is present, so that atmospheric echoes are available for comparison. Figure 2 shows the three facsimile records for each antenna during the event, while in Fig. 3 the statistics of the dot number for each antenna as a function of the height and the total number of dots are shown. The sum of the three signals has been digitized at 1500 Hz using the reference frequency to produce the sampling pulse. To solve ambiguities due to the simultaneous recording of DTEs by two antennas, we have also digitized the three signals separately. Figure 4a gives an example of the DTE signal in the time and frequecy domain. Most of the time the sharp edges allow us to determine the duration accurately. In Fig. 4b the echo from a pilot balloon is shown for comparison. We stress that, while the sharp edges of the echoes allowed us to determine the duration accurately, the shape may vary due to undersampling and target velocity.

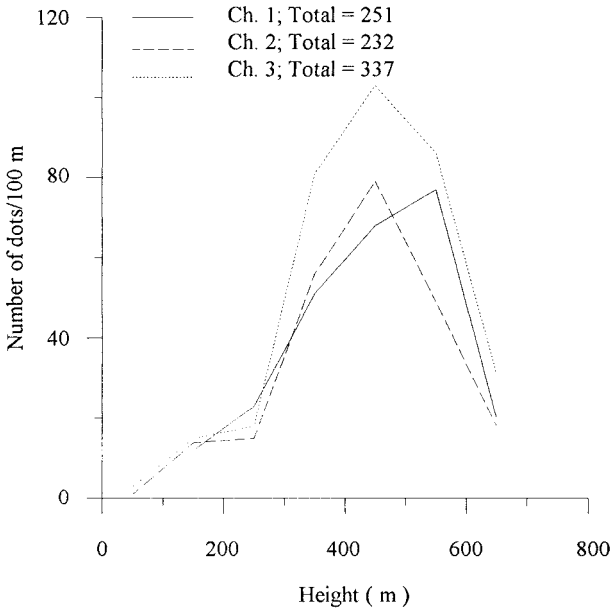

FIG. 3. The number of dot echoes as a function of the height reported for the three channels together with the total number of dots observed in each channel.

a. Target dimensions

The time duration of each DTE was measured in order to estimate the vertical scale of the targets; a summary of the results is presented in Fig. 5. The peak corresponds to a signal time length of 106 ms, which is very close to the nominal 100 ms of the pulse duration. Note that the actual transducer oscillation time (and hence the acoustic pulse) is possibly longer than the electronic triggering pulse due to transducer ringing. The similarity between echo length and output pulse duration implies that the echo has the characteristics of a reflection. The peak in the histogram at 130 ms is due to the simultaneous presence of multiple targets.

Unfortunately, it is not possible to have a direct measurement of horizontal scale using the available data. A rough estimate is possible, however, by assuming that atmospheric targets are homogeneously distributed in the horizontal dimension. If targets are detected simultaneously in two adjacent acoustic beams, we can assume that the beams are overlapping at this height, and the ratio of double-to-single beam detection should be

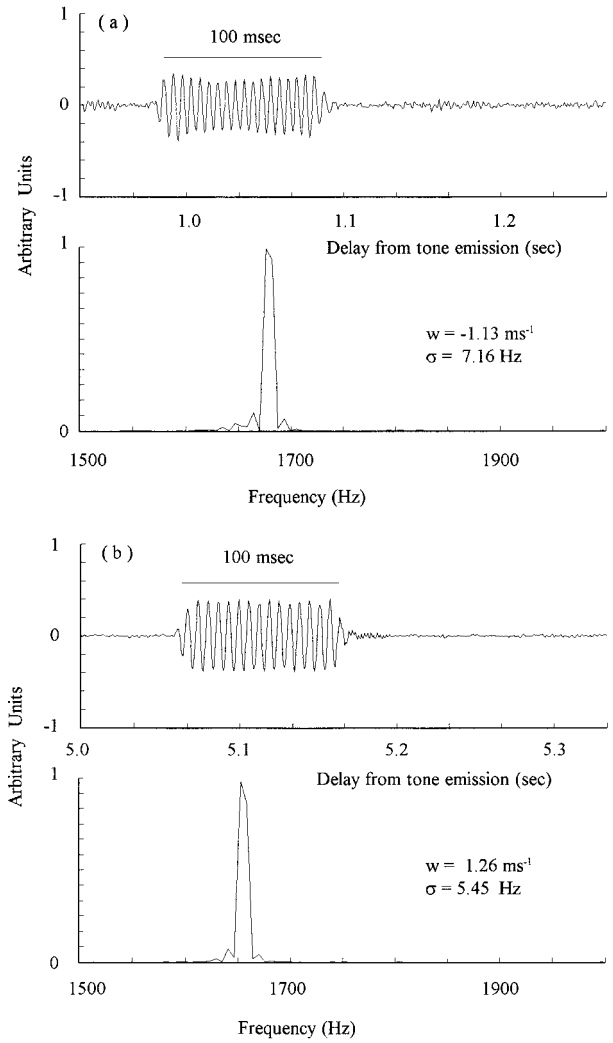

FIG. 4. Digitized signal and related power spectra for (a) dot and (b) pilot balloon echoes. A 100-ms line is reported for comparison. Results of power spectra analysis are also indicated.

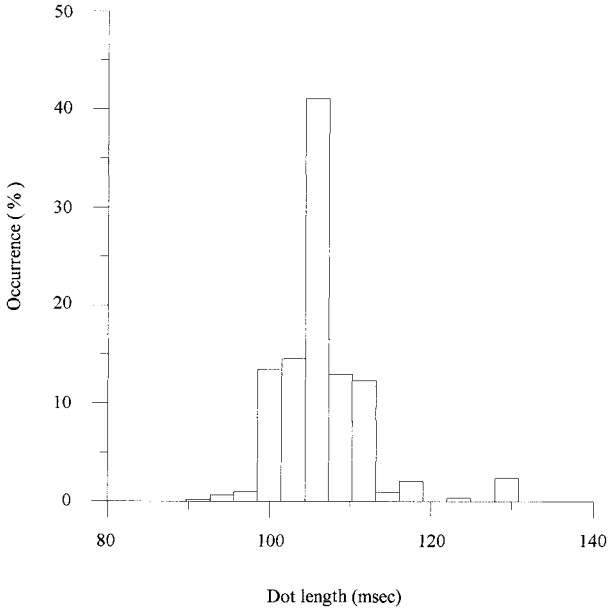

FIG. 5. Histogram of percentage occurrence of dot echo length in terms of time.

proportional to the area of beam overlap normalized by the rest of the beam area at this height. This would be the case only if the targets are sufficiently small. If we neglect the contribution from sidelobes and assume the semiangle of the conical beam to be 1.22 λ/d, where λ is the carrier wavelength and d the antenna diameter, the overlapped area between two beams is given by

$$A_{\mathrm{OV}} = R_1^2(\arccos\vartheta_{1\_2} - 0.5\sin 2\vartheta_{1\_2}) + R_2^2(\arccos\vartheta_{2\_1} - 0.5\sin 2\vartheta_{2\_1}), \quad (1)$$

where R_a is the radius of the beam as a function of the height associated with antenna "a," and

$$\vartheta_{a\_b} = \frac{(D^2 + R_a^2 - R_b^2)}{(2DR_a)}, \quad (2)$$

where D is the distance between the two beam axes; a and b may be equal to 1, 2, or 3. The ratio between the common overlap area (A_{OV}) and the remainder (A) may be compared with the ratio between the cases in which DTEs are simultaneously visible in two beams (D_{OV}) and the number of single DTE episodes (D_a).

If the targets have a significant horizontal dimension, r, in the above formulas "R" becomes "$R + r$." Figure 6 gives the ratio of beam overlap to total beam area as a function of height. The figure titles give the main beam antenna channel (first number) plus the overlapping channel (second number). Three values of target area, r, are plotted: 0 (dotted line); 25 m (broken line), 50 m (continuous line), along with the experimental values. The comparison results do not appear homogeneous for the different beam combinations. This may be due to the lack of homogeneity in the horizontal target distribution, the origin of which is difficult to explain for "atmospheric" targets. We should point out that antenna 2 was located in the middle of a bare land (200 m × 150 m), while antennas 1 and 3 were closer to a cluster of trees. What we can say from comparisons in Fig. 6, however, is that the horizontal dimensions are very likely below 80 m. Actually, if the curve corresponding to 80 m is drawn in the graph, most of the experimental values lie below the curve. If sidelobes have to be taken into account, the expected dimensions should be lower. From the same figure we may notice that below 300 m no DTEs are revealed in the common beam areas.

Target size characteristics may be inferred from the above analysis, which agrees with previous studies. The duration of the DTEs indicate an upper limit to their vertical size of around a few meters (below 10 m). If we look at the shapes of the echoes (sharp edges and very narrow power spectrum; see Fig. 4), they appear

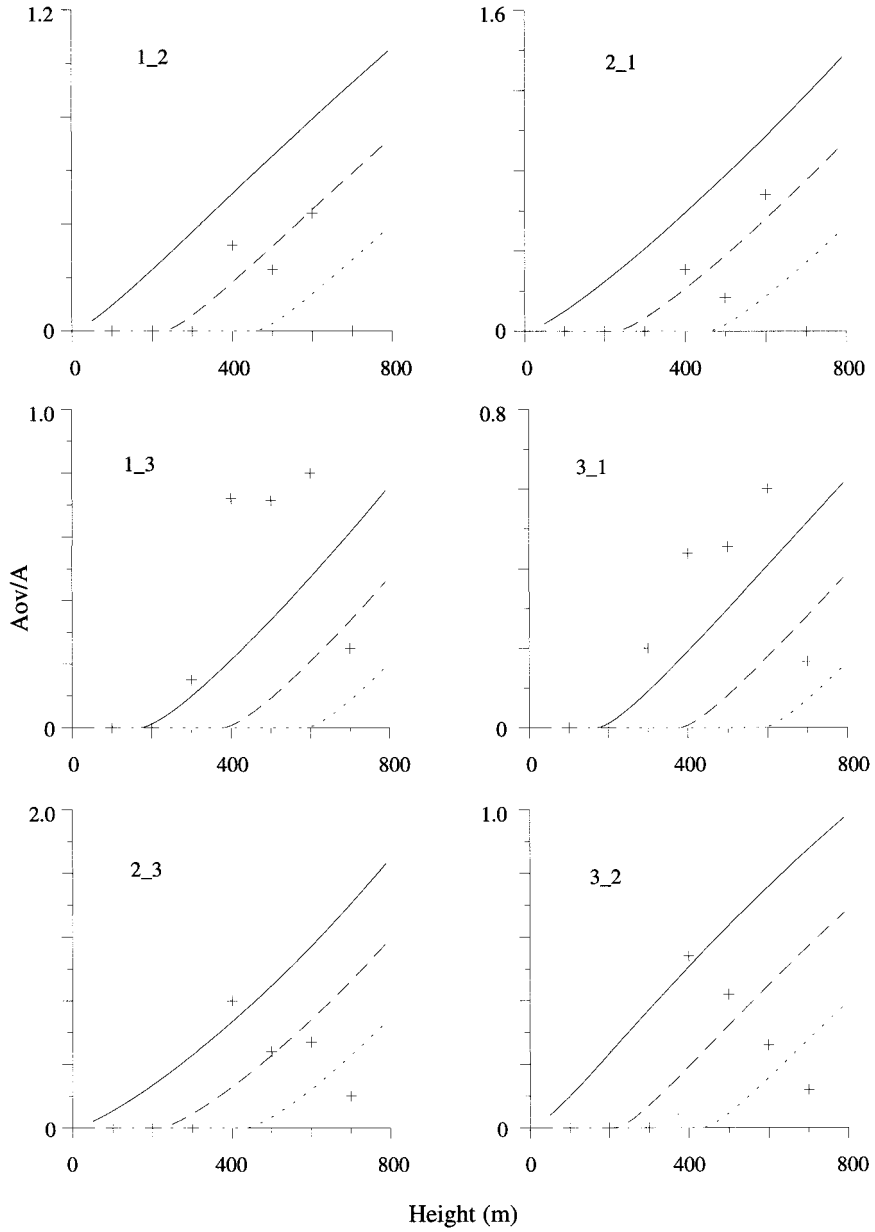

FIG. 6. The rate A_{OV}/A for each antenna beam is plotted as a function of height for three guessed diameters of the target area: 0 (dotted line), 25 (broken line), and 50 m (continuous line). Crosses are the experimental values. The six graphs represent the possible combinations between each channel beam (first number in the title) and the channel with which the common area is shared (second number in the title).

to be due to reflections, as suggested also by Petenko and Kallistratova (1996), who attributed to DTEs vertical sizes much less than 8 m. Similar values are obtained by De et al. (1994; see Fig. 5), while Singal et al. (1985) set an upper limit of 40 m to their vertical extension. Mingyu et al. (1981) observe that the vertical scale is not greater than an acoustic pulse width.

The horizontal dimensions retrieved from our calculations match those obtained by other authors, who based their results on the permanence of dot echo structure in successive scans and on the assumption that the dot structures are translated through the acoustic beam by the mean horizontal wind. Singal et al. (1985) report how the typical horizontal width range is 25–50 m; De et al. (1994) show how the upper limit of their observation is 45 m, while Mingyu et al. (1981) find that the maximum horizontal scale of DTE is 190 m, but most of the values are within 30 m.

We would like to point out that while our results for target dimensions are in agreement with the previous

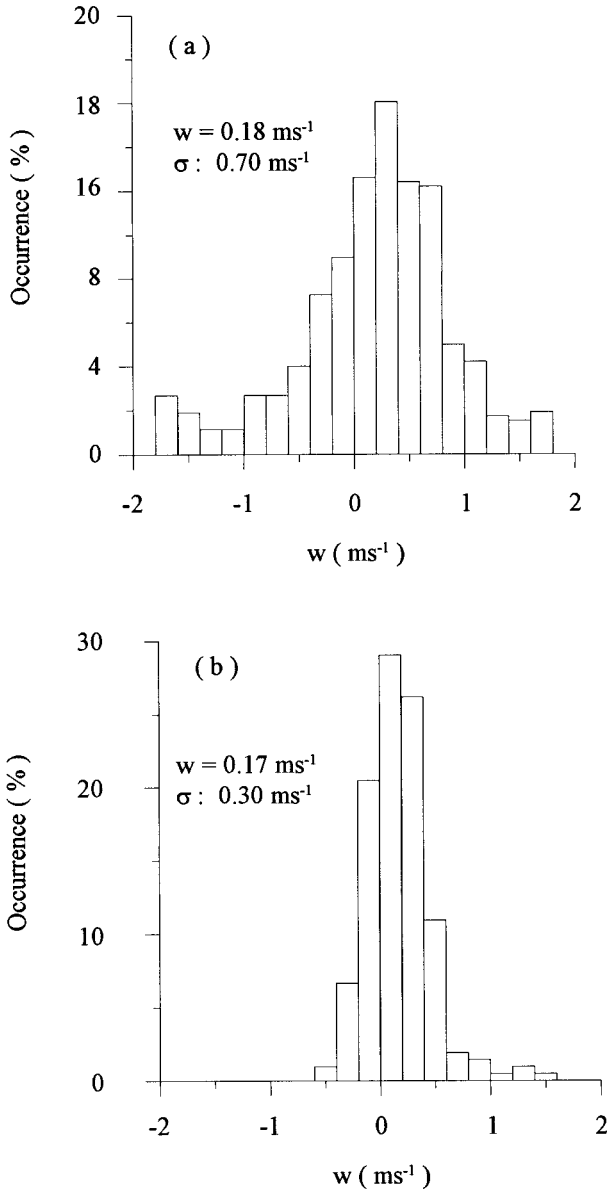

FIG. 7. Percentage occurrence histograms of radial velocity measured for (a) dot echoes and (b) atmospheric echoes.

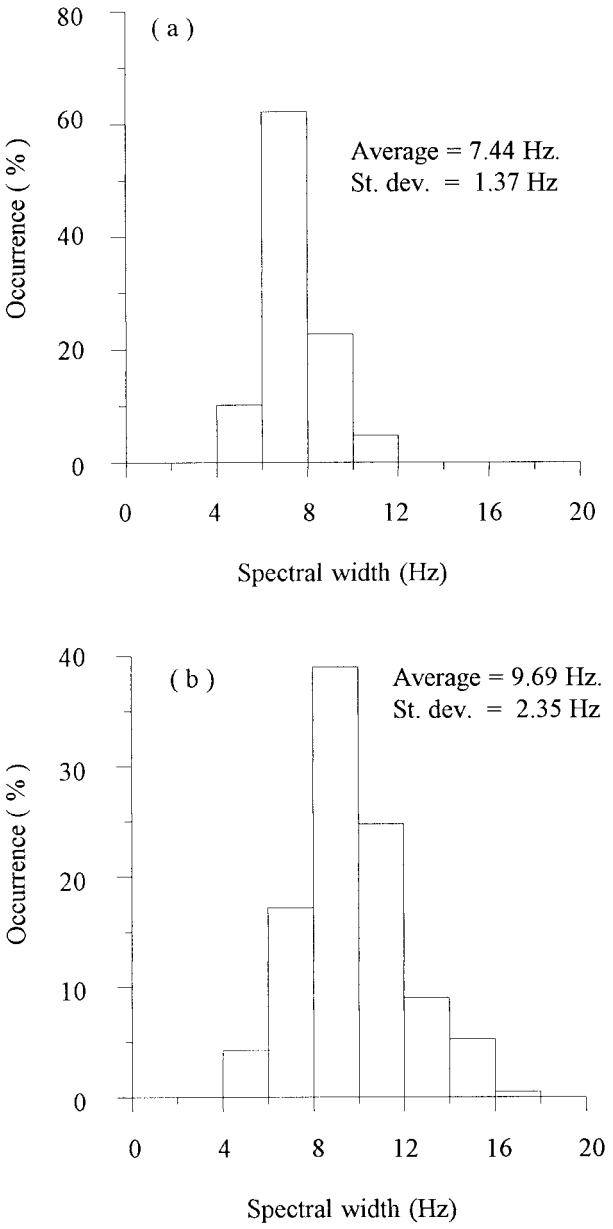

FIG. 8. Percentage occurrence histogram of the spectral width calculated for (a) dot echoes and (b) atmospheric echoes.

ones, the lack of homogeneity in the graphs regarding the different beam axes do not favor our assumption of horizontal homogeneity.

b. Spectral characteristics

In the height range between 300 and 600 m, DTEs seem to be randomly distributed in time and height. In contrast, normal atmospheric echoes visible in the same region have a more layered structure. These will be referred to as stratified atmospheric echoes (SAEs). DTEs and SAEs with a backscatter signal-to-noise parameter (FI) greater than 0.75 are selected (Mastrantonio and Fiocco 1982), and the resulting first- and second-order momenta of the spectra are then calculated. Most of the DTE spectra have FI $>$ 0.85. Figures 7a and 7b show histograms of DTE and SAE vertical velocities, respectively, while Fig. 8 shows their spectral standard deviations. Comparison of first and second power spectrum momenta shows that the dot echoes have a much larger spread of radial velocity than atmospheric backscatter, while their spectral width is smaller. This implies that the dots are not due to any atmospheric effects, such as correlated humidity–temperature variation or reevaporation of water vapor, as suggested by Rao et

al. (1995); such atmospheric sources of acoustic backscatter would be expected to exhibit similar mean velocities to the surrounding air. In this way, all backscatter of atmospheric origin should, in the short term, act as wind vector tracers and give a similar spectral Doppler shift sound. In addition, the standard deviation of the Doppler shift, which indicates the wind velocity perturbation from turbulence, should also be similar. The disparity seen in these data between both mean and standard deviation measurements strongly suggests that the dot echo targets are mobile with respect to the atmosphere.

We note that in Rao et al. (1995), as far as we are aware the only other study that measures the radial velocity of dot echoes, the histogram shows a greater spread in vertical velocity than in this case. Values in excess of 3–4 m s^{-1} (upward and downward) have been recorded, while the background atmospheric vertical velocities lie below 1–2 m s^{-1}. They attribute these large values to the water falling out immediately upon formation and reevaporation.

c. Horizontal velocity

Direct measurements of horizontal target velocity via radar requires three simultaneous measurements of nonparallel Doppler signals. Despite the lack of suitable data in our studies, an estimate of velocity may be made using the following assumptions.

- Targets travel with constant velocity through the beam on a plane perpendicular to the beam axis.
- The targets are randomly distributed and dispersed, such that only one target is in the beam at any one time.

Given the above, the number of successive profiles in which a single dot echo is reproduced is a function of the target velocity v, the period between tone emissions T, and the orthogonal distance between target trajectory and beam axis r. This makes an additional assumption that all targets travel with the same velocity. The number of successive profiles detecting a target is proportional to $L_c/(vT)$, where L_c is the chord length given by

$$L_c = 2(R^2 - r^2)^{1/2}, \quad (3)$$

that is, the length of the target trajectory inside the acoustic beam.

By dividing the entire conic section between 400 and 500 m (where most of the dot echoes are observed) in 200 slices and by summing the probabilities for single or multiple successive dot echoes in each slice, we obtain the probability distributions for different target velocities as a function of the ratio of multiple echoes.

In Fig. 9 these distributions are shown together with the experimental data obtained by summing the single and multiple consecutive appearance of dot echoes in the three antennas. The three-beam radii are approximately equal, and data from all three beams are used to improve the statistics. The resulting distributions do not have the expected single peak, probably due to a lack of horizontal homogeneity in the target distribution. The presence of the higher peak at one single echo probability, which is also detected in the single beam distributions, leads us to the conclusion that target velocity is higher than 4 m s^{-1} (probably close to 16 m s^{-1}). This is significantly greater than the velocity of air at this height, which implies that the targets are moving horizontally with respect to the air. These velocities are clearly not compatible with the background weather conditions that have been previously mentioned.

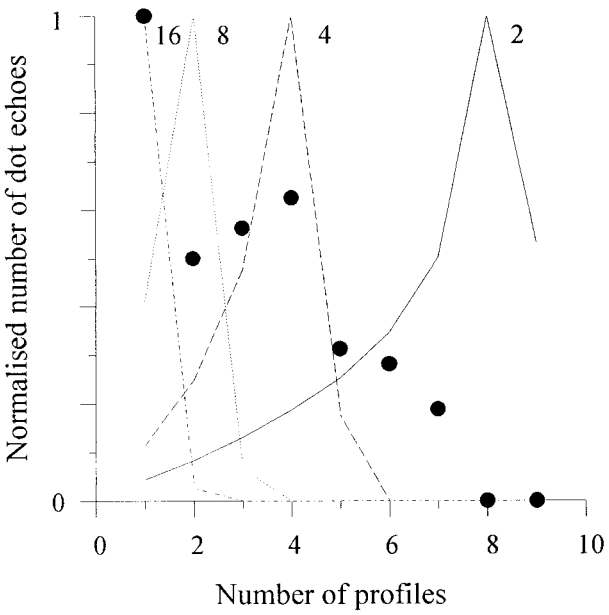

FIG. 9. Normalized expected frequency distributions of the number of single or multiple successive DTEs associated with a single target for several values of horizontal speeds (right of the peaks in m s^{-1}). Filled circles represent experimental values.

4. Comparison among some characteristics of echoes having different origin

A variety of echo structures that can be identified as belonging to atmospheric and nonatmospheric targets were recorded during the Turbigo campaign. This allows us to make a direct comparison between the spectral characteristics of the different echo types.

We have already seen an example of acoustic backscatter from a pilot balloon. The balloons, approximately 1 m in diameter, were occasionally launched during the field work in order to measure wind profile. Shown in Fig. 10a is the echo from a pilot balloon crossing the beam of channel 3. The balloon entered the beam at a height of approximately 680 m and remained visible for 45 scans, equivalent to 4.5 min, before going beyond the range of the instrument. An example of the sampled signal and its Fourier transform is shown in

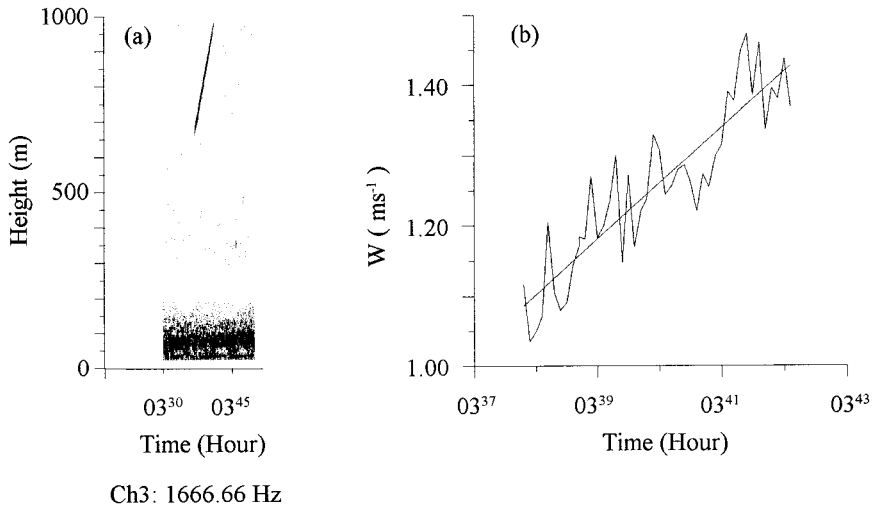

FIG. 10. Trace of a pilot balloon on (a) the channel 3 echogram and (b) the associated radial velocities. The linear trend is due to the horizontal wind profile and to beam width.

Fig. 4b; Fig. 10b gives the resulting values for the vertical velocity *w*. There is an apparent linear trend, possibly due to the wind profile and the finite beamwidth. If the trend is subtracted, we find that the standard deviation σ_w is around 0.05 m s^{-1}. The mean spectral width is 5.6 Hz with a standard deviation of 0.3 Hz.

Figure 11 shows a facsimile record of typical, unusual echoes at around 500–600 m that occurred 5 min after a vertical black line caused by ambient noise. The sodar system was located along the approaching path of the Malpensa airport 14 km to the north; the approaching path was from 348° at the airport. The noise is due to an aircraft approaching the runway. The echoes appearing approximately 5 min later are due to the thermal turbulence as the wake of the airplane passes through an inversion layer. In two cases the echoes have a clearly visible and characteristic aircraft wake signature, while in two other cases they are partially obscured by the noise from successive airplane approaches. Echoes having similar characteristics have been recorded by other authors. Cronenwett et al. (1972), as in our case, showed facsimile records in which several echoes produced by a helicopter vortex drift slowly through the sodar beam approximately 5 min after the noise originated by the helicopter itself. The vortex is postulated to have a diameter of 30 m. The propagation of wakes after the passage of an aeroplane have been also observed with frequency-modulated continuous-wave (FM–CW) radars (Chadwick and Gossard 1986).

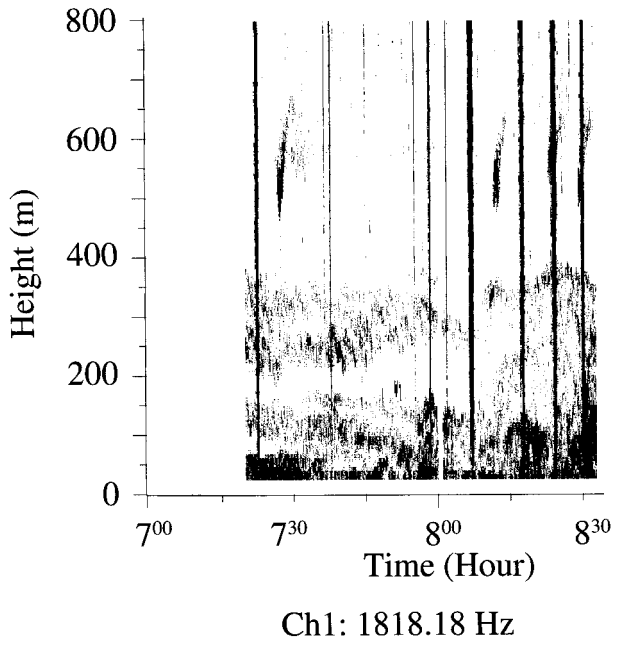

FIG. 11. Noise and echo from wakes caused by airplanes, 6 Sep 1979.

In Fig. 12, echoes are shown from the ENEL (the Italian national electricity board) power plant's exhaust plume located 2 km southwest from the sodar site. The three antenna records indicate the intermittence rate.

In Figs. 13a–d the backscatter power spectra associated with the relevant range gate for a series of 30 successive scans are shown as pseudo-three-dimensional graphs. The four graphs refer to pilot balloon echoes, dot echoes, plume echoes, and wake echoes. The *z*-axis labels are in arbitrary units. In Fig. 13b the 1666.66-Hz backscatter exhibits echo signature associated with inversion layers, but with an intensity much lower than from the dot echoes.

The spectral signatures from the known sources may be compared to that from the dot echo. The dot echo spectral series are most similar to those from the balloon; the extended permanence of the balloon backscatter being due to the slow transect of the target

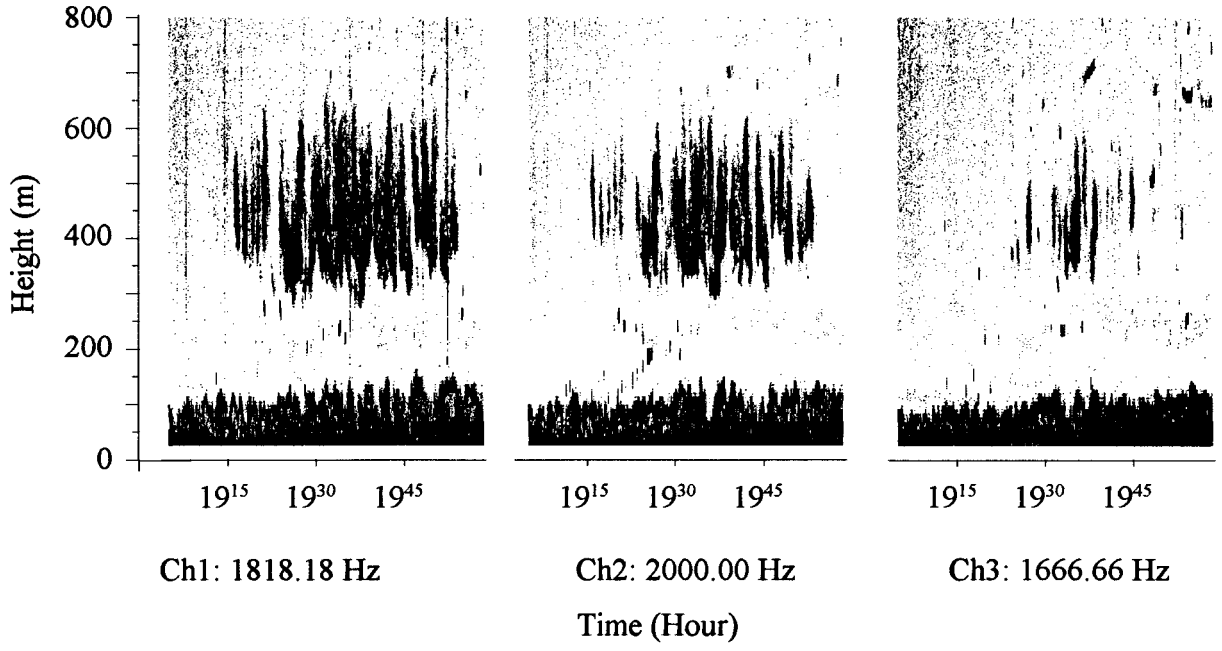

FIG. 12. Echograms recorded by the three antennas on 13 Sep 1979. The intermittent strong echoes between 300 and 600 m are due to exhausted gas plume produced by a power plant. Dot echoes can also be seen.

through the beam. The similarity of the two echo signatures is also evident in Fig. 4. If we compare the mean and standard deviation of dot, pilot balloon, and atmospheric echo spectral widths, we see that dot echoes have values between those from the pilot balloon and atmospheric backscatter. This may be explained by the lack of atmospheric backscatter contamination in the pilot balloon. Alternatively, the spectral spread may be from small-scale movement of the dot echo target, which would be expected from the flapping wings of bird targets; radar signal modulation at bird wingbeat rates has been previously recorded (Vaughn 1985).

The flashlike appearance of the peaks in the spectra, the variation in Doppler frequency between successive scans, and the analysis of the horizontal velocity imply that the dot targets have a velocity that is different from the mean wind speed. In Fig. 13b notice that at scan numbers 7 and 8 two peaks in channel 2 (2000.00 Hz) have Doppler shifts corresponding to -0.50 and 0.95 m s^{-1}, respectively, and two peaks in the scans 12 and 13 have Doppler shifts of -1.3 and 0.6 m s^{-1}, respectively. This rapid change in the vertical velocity is uncharacteristic of backscatter from atmospheric background during fair weather conditions. Isaminger (1995) notes that the spectral width of biological targets is generally less than from turbulent wind shear events.

Although Petenko and Kallistratova (1996) also estimate that the dot echo scattering cross section is close to bird size and hence that dot echoes are due to reflection from birds, they were doubtful about this conclusion because of the lack of confirming visual observation. This may not be counter to a bird-target hypothesis, as birds flying at heights of hundreds of meters are difficult to observe. Larkin (1991) reports how human operators of weather radars seldom identify birds as such and mentions how birds flying at heights greater than 500 m may not be visible even if binoculars are used.

The above analyses show that dot echoes cannot be attributed to atmospheric targets but are due to reflection from solid targets.

5. Conclusions

The discrimination of ''atmospheric'' and ''nonatmospheric'' is a problem that is present in active remote sensing techniques. In the radar meteorology it is widely accepted that birds and insects are the primary cause of dot angels. Several diagnostic variables have been proposed for distinguishing bird and insect echoes since their presence introduces relevant errors in the measurements. A similar problem is present in acoustic remote sensing where anomalous echoes, usually named DTEs, have been noticed by several authors and attributed mostly to humidity–temperature microstructures or to anisotropic irregularities in the lower atmosphere.

In the present paper a detailed analysis of dot echoes has been carried out. To this purpose a dataset recorded by a Doppler sodar with the three antennas pointing vertically has been used. Their characteristics in the time and frequency domain have been analyzed and compared with the more usual atmospheric echoes. It has been demonstrated that the dot echo has the characteristic of a reflection and a horizontal dimension lower

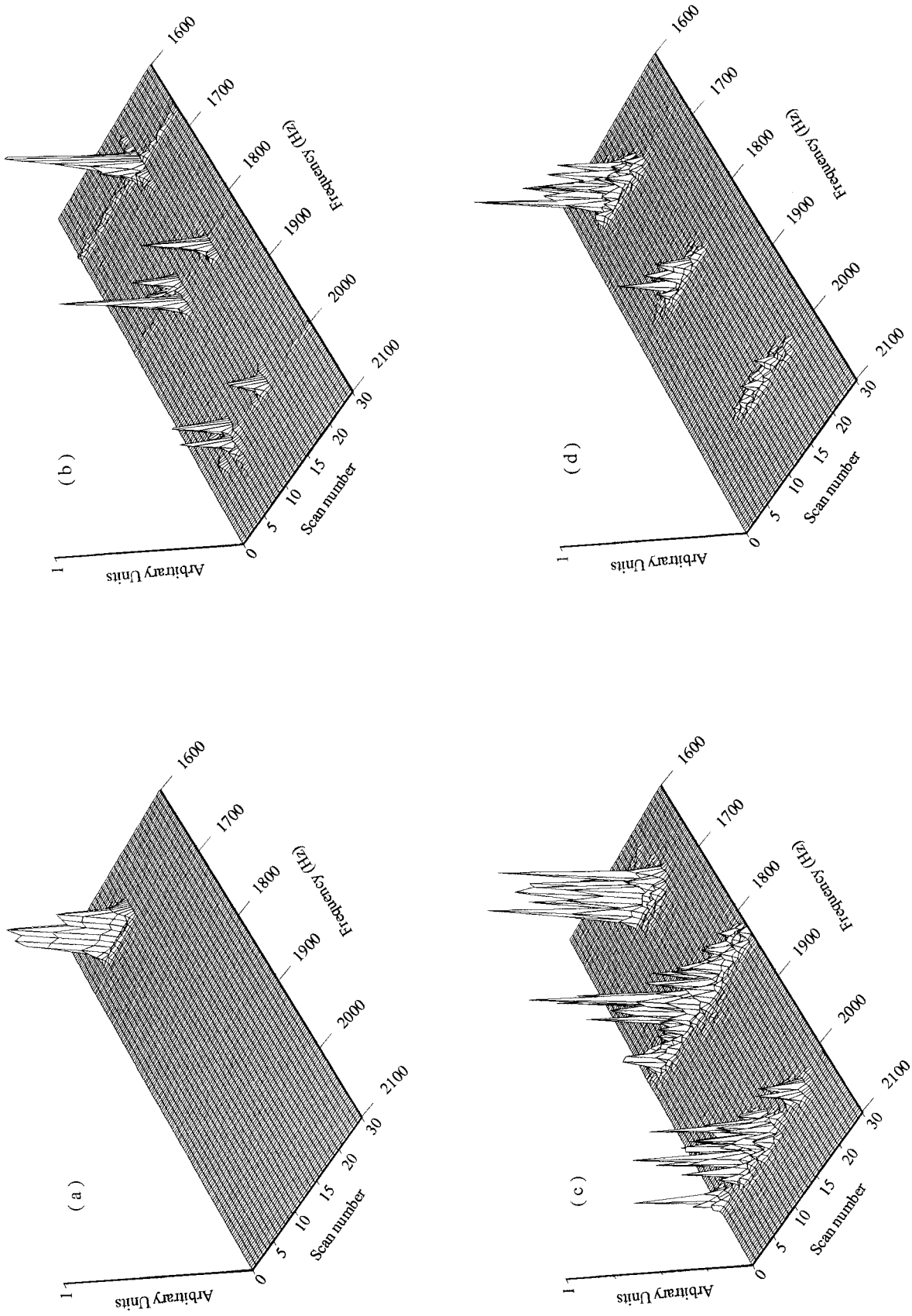

FIG. 13. Backscatter power spectra associated with the relevant range gate for a series of 30 successive scans are shown as pseudo-three-dimensional graphs. The four graphs refer, respectively, to (a) pilot balloon echoes, (b) dot echoes, (c) plume echoes, and (d) wake echoes.

than approximately 80 m. Their spectral characteristics (width and radial velocity) are very different from the ones obtained for usual atmospheric echoes contemporarily detected in the same atmospheric layers. The horizontal velocity, estimated from the number of signature of dot echoes in successive scans close to 16 m s^{-1} is not compatible with the maximum values expected for wind speed in the background atmospheric conditions. Comparisons, in time and frequency domain, have also been made among echoes originated by different targets, recorded in the same dataset: pilot balloons, stack plume, and airplane wake echoes. Dot echoes have characteristics very similar to the ones produced by pilot balloons.

The above analysis clearly indicates that the DTEs cannot have atmospheric origin. The only possible origins are birds and bats since the estimated velocities are larger than the ones usually recorded by radar for insect swarms (Zrnić and Ryzhkov 1998).

Acknowledgments. Financial assistance to one of the authors (JN) by ICTP Programme for Training and Research in Italian Laboratories, Trieste, Italy, is thankfully acknowledged. This research has been partially supported by Italian PNRA and by INTAS through Project 96-1869. The authors thank Prof. G. Fiocco and Dr. A. Ricotta for their contribution in obtaining experimental data.

REFERENCES

Anderson, P. S., 1996: Comparison of internal gravity wave events recorded by sodar and microbarograph over an Antarctic Shelf. *Proc. ISARS,* Moscow, Russia, A. M. Obukhov Institute of Atmospheric Physics, 7.7–7.11.

Argentini, S., G. Mastrantonio, A. Viola, P. Pettré, and G. Dargaud, 1996: Sodar performance and preliminary results after one year measurements at Adelie land coast, east Antarctica. *Bound.-Layer Meteor.,* **81,** 75–103.

Battan, L. J., 1973: *Radar Observation of the Atmosphere.* 2d ed. University of Chicago Press, 323 pp.

Caccamise, D. T., and J. Fischl, 1985: Patterns of association of secondary species in roosts of European starlings and common grackles. *Wilson Bull.,* **97,** 173–182.

Chadwick, R. B., and E. E. Gossard, 1986: Radar probing and measurement of the planetary boundary layer. Part I: Scattering from refractive index irregularities. *Probing the Atmospheric Boundary Layer,* D. H. Lenshow, Ed., Amer. Meteor. Soc., 163–182.

Cronenwett, T. W., G. B. Walker, and R. L. Inman, 1972: Acoustic sounding of meteorological phenomena in the planetary boundary layer. *J. Appl. Meteor.,* **11,** 1351–1358.

De, A. K., S. Tripathy, and J. Das, 1994: On fine structure of dot echoes as observed by acoustic sounder. *Int. J. Remote Sens.,* **15,** 2157–2165.

Drake, V. A., 1982: Insects in the sea-breeze front at Camberra: A radar study. *Weather,* **37,** 134–143.

Eastwood, E., 1967: *Radar Ornithology.* Methuen and Co., Ltd., 278 pp.

Fiocco, G., and G. Mastrantonio, 1983: Characters of the air flow inferred from detailed spectral analysis of acoustic sounder echoes. *J. Acoust. Soc. Amer.,* **74,** 1861–1865.

——, G. Mastrantonio, and A. Ricotta, 1980: Boundary layer structure observed by shipborne Doppler sodar in the Suez Canal zone. *Nuovo Cimento,* **3C,** 321–344.

Gauthreaux, S. A., Jr., 1980: Direct visual and radar methods for the detection, quantification and prediction of bird migration. Spec. Publ. No. 2, Dept. Zool., Clemson University, Clemson, SC, 67 pp. [Available from Department of Zoology, Clemson University, Clemson, SC 29634.]

Gaynor, J. E., and P. A. Mandics, 1978: Analysis of the tropical marine boundary layer during GATE using acoustic sounder data. *Mon. Wea. Rev.,* **106,** 223–232.

Greenbank, D. O., C. W. Schaeler, and R. C. Rainey, 1980: Spruce Budworm (Lepidoptera; Tortricidae) moth flight and dispersal: New understanding from canopy observations, radar and aircraft. *Mem. Entomol. Soc. Can.,* **110,** 1–49.

Greenhut, G. K., and G. Mastrantonio, 1989: Turbulence kinetic energy budget profiles derived from Doppler sodar measurements. *J. Appl. Meteor.,* **28,** 99–106.

Hardy, K. R., and I. Katz, 1969: Probing the clear atmosphere with high power, high resolution radar. *Proc. IEEE,* **57,** 468–480.

Isaminger, M. A., 1995: Techniques for discriminating biological targets from wind shear events using Doppler radar and atmospheric soundings. Preprints, *27th Int. Conf. on Radar Meteorology,* Vail, CO, Amer. Meteor. Soc., 659–662.

Jungbluth, K., J. Belles, M. Schumacher, and R. Arritt, 1991: Velocity contamination of WSR-88D and wind profiler data due to migrating birds. Preprints, *25th Int. Conf. on Radar Meteorology,* Paris, France, Amer. Meteor. Soc., 666–668.

Larkin, R. P., 1991: Sensivity of NEXRAD algorithms to echoes from birds and insects. Preprints, *25th Int. Conf. on Radar Meteorology,* Paris, France, Amer. Meteor. Soc., 203–205.

——, and D. Q. Quine, 1987: Draft report on bird movement data. *Illinois Natural History Survey, Section on Wildlife Research,* University of Illinois, 78 pp.

——, and ——, 1989: Report on Bird Hazard Algorithm. *Illinois Natural History Survey, Section on Wildlife Research,* University of Illinois, 73 pp.

Lee, R. L., J. L. Ingram, and G. E. Klazura, 1995: A comparision of data from the WSR-00D VAD wind profiler product and rawinsondes at twelve sites. Preprints, *27th Int. Conf. on Radar Meteorology,* Vail, CO, Amer. Meteor. Soc., 663–665.

Mastrantonio, G., and G. Fiocco, 1982: Accuracy of wind velocity determinations with Doppler sodar. *J. Appl. Meteor.,* **21,** 820–830.

——, and S. Argentini, 1997: A modular PC-based multiband sodar system. *Acoustic Sounding and Applications,* S. P. Singal, Ed., Narosa Publishing House, 105–116.

——, and Coauthors, 1994: Aspect of low level circulation in the Tiber valley as observed with a sodar network. *Bound.-Layer Meteor.,* **71,** 67–80.

Mingyu, Z., L. Naiping, C. Yanjuan, and L. Shiming, 1981: The lump structure of turbulent field in atmospheric boundary layer. *Scientia Sinica,* **24,** 1705–1716.

O'Bannon, T. D., 1995: Anomalous WSR-88D wind profiles—Migrating birds? Preprints, *27th Int. Conf. on Radar Meteorology,* Vail, CO, Amer. Meteor. Soc., 663–665.

Ottersten, H., 1970: Radar angels and their relationship to meteorological factors. FOA Reports 4, No. 2, Research Institute of National Defense, Sweden, 33 pp.

Parry, H. D., M. J. Sanders, and H. P. Jensen, 1975: Operational applications of a pure acoustic sounding system. *J. Appl. Meteor.,* **14,** 67–77.

Pedgley, D. E., D. R. Reynolds, J. R. Riley, and M. R. Tucker, 1982: Flying insects reveal small-scale wind systems. *Weather,* **37,** 295–306.

Petenko, I. V., and M. A. Kallistratova, 1996: Dash echo structures as observed by acoustic sounding. *Proc. ISARS,* Moscow, Russia, A. M. Obukhov Institute of Atmospheric Physics, 6.109–6.114.

Rao, M. P., S. Casadio, G. Fiocco, F. Lena, M. Cacciani, P. G. Calisse, A. di Sarra, and D. Fua, 1995: Observation of lump structures in the nocturnal atmospheric boundary layer with Doppler sodar and Raman lidar. *Geophys. Res. Lett.,* **22,** 2505–2508.

Reynolds, D. R., 1988: Twenty years of radar entomology. *Antenna,* **12,** 44–49.

Richardson, W. J., 1976: Bird migration over southeastern Canada, the western Atlantic and Puerto Rico: A radar study. Ph.D. dissertation, Cornell University, 1074 pp. [Available from University Microfilm, 305 N. Zeeb Rd., Ann Arbor, MI 48106.]

Riley, J. R., 1989: Remote sensing in entomology. *Ann. Rev. Entomol.,* **34,** 247–271.

——, 1994: Acoustic sounding, atmospheric structure and insects. *Int. J. Remote Sens.,* **15,** 293–297.

——, and D. R. Reynolds, 1979: Radar-based studies of the migratory flight of grasshoppers in the middle Niger area of Mali. *Proc. Roy. Soc. London B,* **204,** 67–82.

Singal, S. P., B. S. Gera, and S. K. Aggarwal, 1985: Studies of sodar observed dot echo structures. *Atmos.–Ocean,* **23,** 304–312.

Skolnik, M. I., 1970: *Radar Handbook.* McGraw Hill, 1200 pp.

Vaughn, C. R., 1985: Birds and insects as radar targets: A review. *Proc. IEEE,* **73,** 205–227.

Vetrov, V. I., and Y. N. Ulianov, 1996: A dot echo investigation with sodar and RASS techniques. *Proc. ISARS,* Moscow, Russia, A. M. Obukhov Institute of Atmospheric Physics, 6.115–6.119.

——, ——, and V. Bedin, 1998: Formation features and the fine structure of sodar dot-echoes. *Proc. ISARS,* Vienna, Austria, Institute for Meteorology and Physics, BOKU, 115–118.

Wilczak, J. M., and Coauthors, 1995: Contamination of wind profiler data by migrating birds: Characteristics of corrupted data and potential solutions. *J. Atmos. Oceanic Technol.,* **12,** 449–467.

William, T. C., and Coauthors, 1972: Tracking radar studies of bird migration. *Animal Orientation and Navigation,* S. R. Galler et al., Eds., NASA SP-262, 115–128.

Zrnić, D. S., and A. V. Ryzhkov, 1998: Observations of insects and birds with a polarimetric radar. *IEEE Trans. Geosci. Remote Sens.,* **36,** 661–668.